



Reactive sintering: An important component in the combustion of nanocomposite thermites

K.T. Sullivan^a, N.W. Piekielek^a, C. Wu^a, S. Chowdhury^a, S.T. Kelly^b, T.C. Hufnagel^b, K. Fezzaa^c, M.R. Zachariah^{a,*}

^aUniversity of Maryland, College Park, MD 20742, United States

^bJohns Hopkins University, Baltimore, MD 21218, United States

^cAdvanced Photon Source, Argonne National Laboratory, Argonne, IL 60439, United States

ARTICLE INFO

Article history:

Received 9 March 2011

Received in revised form 19 May 2011

Accepted 25 July 2011

Available online 19 September 2011

Keywords:

High heating

Thermites

Aluminum

Phase contrast imaging

Microscopy

Nanoparticles

ABSTRACT

One of the open questions in understanding the reactivity of nanometric metal/metal oxide particulate composites is the relative role of gas–solid vs. condensed state reactions. This work is an investigation of several nano-Al based thermites subjected to very rapid heating rates. The ignition temperature of thermites, as measured by the onset of optical emission, was measured using a rapidly heated Pt wire. Generally, ignition was seen to occur above the melting temperature of aluminum. The exception was Al/Bi₂O₃ which ignited slightly below this point. Samples were also rapidly heated in situ within electron microscopes to provide direct imaging before and after heating. The sintering of aggregated and/or agglomerated particles into characteristically larger structures was experimentally observed in all cases, and the fuel and oxidizer were found to be in surface contact suggesting that a condensed-phase reactive sintering mechanism had occurred. High resolution image sequences of thermites ignited on the Pt wire were collected using a real time phase contrast imaging technique at the Advanced Photon Source of Argonne National Lab. The results suggest that reactive sintering occurs on a fast timescale, and relatively early in the reaction, leading to rapid melting and coalescence of aggregated particles. This dramatically changes the initial size and morphology of the constituents before the remainder of the material burns. The results question the idea that a decrease in particle size will necessarily lead to an enhancement in reactivity, since large amounts of sintering occurs early in the reaction, and alters the morphology. It is suggested that improvements in reactivity can be achieved by designing architectures to improve the interfacial contact upon sintering, as well as by selecting oxidizers based on their ability to liberate and transport oxygen in the condensed phase, while producing volatile species to assist in convective energy transport.

© 2011 Published by Elsevier Inc. on behalf of The Combustion Institute.

1. Introduction

Nanocomposite thermites, or metastable intermolecular composites (MICs) are intimate mixtures of metal/metal oxide nanoparticles, and typically have the consistency of a loose powder. Using nanoparticles greatly reduces mass diffusion lengths between the fuel and oxidizer, and also increases the interfacial contact and homogeneity of mixing. Upon ignition, these materials give rise to a self-propagating reaction with a characteristically high temperature, and low to moderate gas production. Research on MICs can be traced back about 15 years to when Aumann et al. [1] showed that using nanoparticles of Al/MoO₃ resulted in several orders of magnitude increase in combustion characteristics over similar mixtures with micron-sized particles.

Since then, research efforts have increased to understand the ignition and combustion mechanism, so that improvements in safety and performance can be achieved.

MICs have been experimentally shown to exhibit pressures and flame velocities somewhere in between propellants and explosives [2]. Flame velocities range between 10's to 1000's of meters per second, while the pressures range between a few to nearly 1000 atmospheres. The pressure and flame velocity in MICs is something that can be tuned through easily-adjusted parameters, such as changing the method and uniformity of mixing [3–5], particle size and distribution [6–8], choice of materials and stoichiometry [9], mixture density [10], or by other techniques such as electrostatic assembly [11] or creating new types of core–shell oxidizers [12]. This tunability, along with other attributes such as high mass/volumetric energy densities and the production of environmentally benign products, make MICs very attractive energetic systems. Nano-sized aluminum is a fuel which exhibits a high reactivity,

* Corresponding author. Fax: +1 301 314 9477.

E-mail address: mrz@umd.edu (M.R. Zachariah).

and nano-Al based MICs are currently being investigated for uses in propellants, explosives, and pyrotechnics, along with other more recent applications, such as antimicrobial energetic systems designed to combat harmful biological agents [13].

Despite the amount of experimental results available in the literature, the ignition and combustion mechanism remains poorly understood. A major problem has been designing experimental techniques which can probe the intrinsic reaction while replicating the environment these materials are subjected to during the self-heating in a freely propagating reaction. This means very rapid and uniform heating, speculated to be somewhere in the range of 4×10^4 K/s (Martirosyan et al. [14]) to upwards of 10^8 K/s, predicted by an ad hoc calculation assuming thermites can reach an ignition temperature of ~ 1000 K in 10 μ s, an experimentally observed pressure rise time [15]. Furthermore, in order to understand the thermite mechanism, the ignition and combustion mechanism of nano-Al itself must first be well understood.

Nano-Al forms a passivating oxide shell when exposed to air. This shell is amorphous and uniform [16], and typically has a thickness of 2–3 nm [17]. The oxide shell can occupy a relatively large portion of the particle's mass, and in some cases can even exceed 50 Wt% [18]. One result generally observed is that the measured ignition temperature of nano-Al is much closer to the melting point of Al, and far below the melting point of Al_2O_3 , which is where large aluminum is reported to ignite [17]. This observation has led to much speculation that the interaction between the low melting point core (933 K) and the high melting point shell (2327 K) is critical to elucidate the underlying mechanism leading to ignition.

Several authors have focused on understanding the ignition mechanism of nano-Al from the standpoint of the core/shell interaction. Trunov et al. [17,19] used thermal analysis (~ 40 K/min) and developed an ignition mechanism suggesting that outwards transport of aluminum can occur as the oxide shell undergoes polymorphic phase transformations, rendering it permeable to aluminum. Using hot stage microscopy at similar heating rates and under vacuum, Rai et al. [20] have observed the outwards flow of aluminum through the oxide shell above the melting temperature. In a separate work, it was shown using molecular dynamics simulations that the effective transport rate of aluminum through the shell can significantly be enhanced by built-in electric fields [21]. At even higher heating rates ($\sim 10^6 - 10^8$ K/s), Levitas et al. [22–25] have suggested that a “Melt Dispersion Mechanism” can occur. In such a mechanism, the rapid melting of the aluminum core induces significant stress in the oxide shell to completely rupture it, followed by the subsequent unloading of the aluminum core via tensile stresses. The authors have suggested that in such a mechanism, the kinetics would not be limited by diffusion. A key parameter for this mechanism is the relative thickness of the oxide shell to the aluminum core, and the authors have shown in some cases that increasing the shell thickness can lead to a higher flame velocity, a result which is consistent with such a mechanism.

Understanding the oxidation mechanism of nano-Al is even more challenging when one considers that the mechanism is strongly contingent upon understanding the relevant ignition mechanism. Also, experimental techniques which employ uniform and rapid heating rates are necessary to replicate a true combustive environment. Rai et al. [27] have investigated nano-Al oxidation at intermediate heating rates ($\sim 10^3$ K/s) using a furnace, and have suggested that oxidation is diffusion-controlled via a shrinking core mechanism [28], which involves inwards diffusion of O_2 through the oxide shell. At even higher heating rates, ($\sim 10^6 - 10^8$ K/s), Bazyn et al. have conducted several experiments of nano-Al burning in varying environments inside a shock tube [29]. The authors used optical pyrometry to measure the combustion temperature of the particles as a function of pressure and gas composition, and suggest that the burning cannot be modeled by a

droplet burning model, but instead large heat losses characteristic of nanoparticles cause the flame to sit much closer, if not directly on the particle surface. This suggests that heterogeneous reactions between the gas and the particle are prominent in the combustion mechanism. The authors have also investigated the ignition and combustion of nanocomposite $\text{Al}/\text{Fe}_2\text{O}_3$ and Al/MoO_3 using the same technique, and measured the ignition temperatures in an inert environment to be 1400 and 1800 K, respectively [30]. It should be noted that these ignition temperatures are significantly higher than the melting temperature of Al, which has been experimentally observed to be approximately where nano-Al ignites in a gaseous oxidizing environment [17]. The authors also measure the combustion temperatures of the composites to be in the range of 2750–3350 K, and find that combusting in an oxygenated environment can raise the temperature several hundred degrees, indicating some degree of reaction with the gas.

Besides the aforementioned experiments, there have been limited other studies of the ignition and combustion of nano-Al and nano-Al composite materials which:

- (a) Avoid the negative effects of studying a bulk sample such as packing density, mixing, differences in heating, etc.
- (b) Probe intrinsic properties.
- (c) Uniformly and rapidly heat the samples.

These considerations have led to the development of temperature jump (T-Jump) techniques, which can ramp the temperature of a small amount of sample very quickly. In these experiments, a thin wire or filament (coated with sample) is supplied a tunable voltage pulse and rapidly heats ($\sim 10^5 - 10^6$ K/s) through resistive heating. The ignition and combustion event can be monitored optically [31,32], or in a mass spectrometer [33] to probe transient species evolution. Chowdhury et al. [31] used this setup to examine the ignition delay in a nano-Al/CuO composite as a function of aluminum oxide shell thickness. The authors concluded that the diffusion of Al through the oxide shell was responsible for the delay, since an increasing delay time was measured with increasing oxide shell thickness.

One other phenomenon which has received little attention in nanoparticle combustion studies, and is relevant to this work, is the sintering of aggregated particles. This directly impacts the question of size dependence on reactivity, and what is the “effective” particle size of the reacting material. Commercially available nanoparticles are almost always highly aggregated, and the size specified by a supplier often corresponds to the average size of the primary particles within these aggregates. Surface tension forces will of course drive the particles to coalesce if the temperature is sufficiently high to make the particles liquid-like [34,35]. In a reacting thermite, nanoparticles can be rapidly heated by hot interstitial gases, and can be further heated by the energy liberated during an exothermic reaction. If the exothermic reaction is primarily responsible for inducing the sintering processes, it can be referred to as reactive sintering, a phenomenon which has been shown to be important in Al/Ni reacting systems [36].

One key point we will have to consider is how the kinetic timescale for sintering compares with reactive timescales we observe experimentally. If sintering occurs on a comparable timescale, or faster, than the chemical reaction, it raises two very important questions:

- 1) Do nanoparticles maintain their high surface area morphology during combustion, and if not, then what is the appropriate “size” to report?
- 2) Is there an advantage of using aggregated nanoparticles below a certain critical size?

The current work is a compilation of various experiments investigating the reaction mechanism of both nano-Al and nano-Al thermites. The studies are all performed at high heating rates ($10^5 - 10^6$ K/s), by passing a tunable voltage pulse through either a thin Pt wire or a specially fabricated electron microscopy grid. Several different thermite systems were investigated, and not all were studied using every experimental technique, largely due to time constraints on borrowed equipment or facility usage. The particular thermite studied in each case, therefore, was selected based on what would give the clearest representation of the steps involved in the nanocomposite thermite reaction for the particular experimental technique. The experimental results will suggest that a general similarity for all systems studied is that at least some amount of condensed-phase reaction and sintering occurs.

2. Experimental

The nano-Al used in this work is termed “50 nm ALEX”, and was purchased from the Argonide Corporation. The average primary particle size is specified by the supplier to be 50 nm, and the elemental portion of the particles was found to be 70% by mass, measured using thermo gravimetric analysis (TGA). A representative image of the nano-Al is shown in Fig. 1. The primary particles are largely spherical in nature, and are highly aggregated. One of the samples of CuO, which we term “6nmCuO”, was synthesized by a wet chemical technique (using copper nitrate and sodium hydroxide), and the primary particle diameter was found by electron microscopy to be ~ 6 nm. A representative image of the as-prepared material is shown in Fig. 2. The particles are spherical and relatively monodisperse, with varying degrees of aggregation. All other oxidizers were purchased from Sigma Aldrich, and were spherical and aggregated. These include Bi_2O_3 (90–210 nm), WO_3 (<100 nm), Fe_2O_3 (<50 nm), and CuO (<50 nm), with the sizes specified by the supplier. A summary of all materials used is provided in Table 1.

To prepare thermites, stoichiometric amounts of the nano-Al and oxidizer were weighed and added to either a ceramic crucible or glass vial along with a few milliliters of hexane. The samples were then placed into a sonicating bath, followed by ultrasonication for ~ 30 min to ensure intimate mixing. For the wire experiments, the hexane/sample mixture was directly pipetted onto the wire, and the hexane was allowed to evaporate before testing. To prepare the grids for microscopy, the hexane was first allowed to evaporate completely, and then a small amount of ethanol was added to pipette the sample onto the grid. Ethanol was simply chosen based on experience that it evaporated more readily from the microscopy grids.

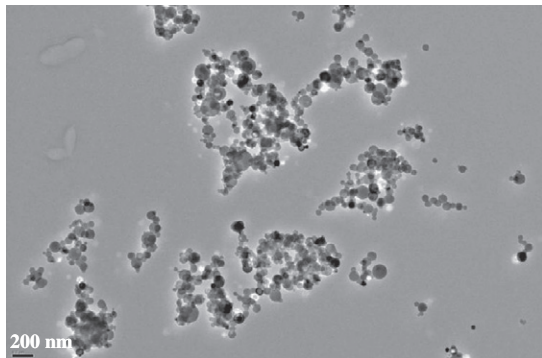


Fig. 1. Representative transmission electron microscope image of “ALEX” nano-Al. The particles have an average primary diameter of 50 nm as specified by the supplier. A native passivating oxide shell with a thickness of 2–5 nm is also present, though it cannot be resolved at this magnification.

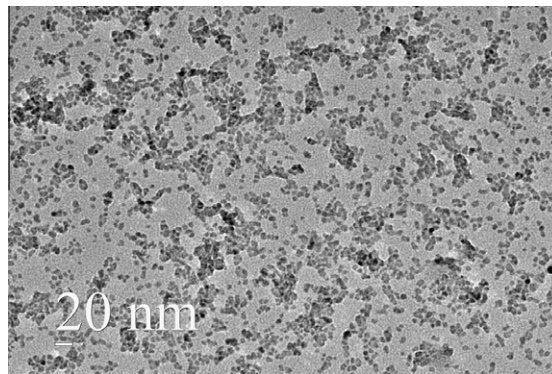


Fig. 2. Representative TEM image of the as-prepared CuO. The primary particle size is ~ 6 nm, as measured by TEM. The particles are spherical with varying amounts of aggregation. A higher resolution image of the CuO can be seen in Fig. 4c.

Table 1

A summary of the materials used in this work. The sizes were all as-specified by the supplier except for the synthesized 6nmCuO, where the size was measured by TEM.

Material	Source	Size (primary particle)
Nano-Al (70% Al, 30% Al_2O_3 measured by TGA)	Argonide Corp.	50 nm
6nmCuO	Prepared by wet chemical synthesis	6 nm (TEM)
CuO	Sigma Aldrich	<50 nm
Fe_2O_3	Sigma Aldrich	<50 nm
WO_3	Sigma Aldrich	<100 nm
Bi_2O_3	Sigma Aldrich	90–210 nm

Three separate experiments were conducted in this work, and as previously mentioned, not all samples were tested using each experiment. The first used a temperature jump (T-Jump) setup to investigate the ignition temperature of the thermite sample rapidly heated on a thin wire in air. The wire is made of Pt, with a diameter of 76 μm , and through utilization of a tunable voltage pulse, can be resistively heated to a high temperature (~ 1500 K) at a rate of approximately 5×10^5 K/s [31,33]. A photomultiplier tube (PMT) is used to monitor the optical emission, and ignition is said to have occurred at the onset of the emission. An example of the data produced by this method is shown for an Al/CuO thermite in Fig. 3. Secondly, a specially designed holder (Aduro holder, Protochips, Inc.) was used to heat samples with a tunable heating

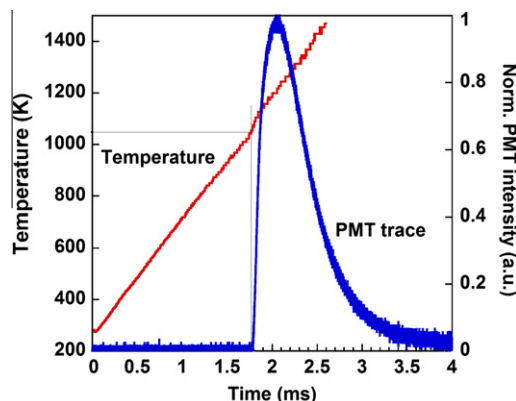


Fig. 3. Typical experimental data for determining the ignition temperature of a thermite (nano-Al/CuO) on a rapidly heated Pt wire. The temperature is calculated for the wire based on resistivity, and the ignition temperature is measured at the onset of optical emission as measured by a PMT.

Table 2

Summary of the thermite systems studied by several different high heating experimental techniques. TEM and SEM are transmission and scanning electron microscope, respectively.

Material or thermite	T-Jump/PMT setup for ignition temp.	T-Jump/movie at APS	High heating TEM (JEOL JEM 2100 LaB6 TEM)	High heating SEM (Hitachi SU-70 SEM)
Nano-Al	No	Yes	Yes	No
Nano-Al/6nmCuO	Yes	No	Yes	No
Nano-Al/CuO	Yes	Yes	No	No
Nano-Al/Fe ₂ O ₃	Yes	Yes	No	No
Nano-Al/WO ₃	Yes	No	No	Yes
Nano-Al/Bi ₂ O ₃	Yes	No	No	No
CuO	N/A	Yes	No	Yes
Fe ₂ O ₃	N/A	Yes	No	No

pulse in situ inside an electron microscope, from room temperature up to a maximum of 1473 K and at a rate as fast as $\sim 10^6$ K/s. The holder can be held at the desired temperature for a user-specified amount of time before being shut off. Pure nano-Al, Al/6 nm CuO, and Al/WO₃ thermites were studied using this holder inside either a scanning (SEM, SU-70 Hitachi Inc.) or transmission (TEM, JEM 2100 Lab6, JEOL Ltd.) electron microscope. Images before and after heating are compared to draw conclusions about the mechanism. Finally, X-ray phase contrast imaging experiments were performed at the Advanced Photon Source (APS). We took the T-Jump system to APS, where a coherent X-ray beam was used to view the thermites rapidly heated on the Pt wire in real time at a frame rate of 135,780 Hz (7.4 μ s per frame). The per-frame exposure time was actually much shorter ~ 500 ns, and was controlled by the pulse width of the synchrotron bunch structure. The high coherence of the undulator X-ray source at APS means that the relative phase of the X-rays (and not simply differential X-ray absorption) contributes to image contrast, making this technique extremely sensitive to gradients in electron density [37]. In addition, the PMT setup was simultaneously used to monitor the optical emission, thus providing a correlation between the images and the emission of light. The various thermites studied, along with which experimental techniques were used, are summarized in Table 2.

3. Results and discussion

3.1. T-Jump/PMT ignition temperature

The ignition temperature, is summarized for various thermite systems in Table 3. Also included in the table is the bulk melting point of the oxidizer. While both WO₃ and Bi₂O₃ do melt, the melting of CuO and Fe₂O₃ involves the decomposition to Cu₂O and Fe₃O₄ (and FeO at higher T), coupled with the release of O₂ gas. We have recently argued, through temporally resolved mass spectrometry, that the O₂ release for these particular oxidizers plays an important role in the ignition and combustion processes [38]. Upon rapid heating, a critical partial pressure of gaseous oxygen may be achieved, which facilitates the ignition of the aluminum fuel. This

Table 3

A comparison of the ignition temperature measured for various thermites and the melting temperature of the metal oxide. The ignition temperature was measured using the rapidly heated Pt wire experiment and monitoring the onset of optical emission via a photomultiplier tube.

Thermite	Ignition temperature (K) \pm 40 K	Oxidizer melting temperature (bulk values) (K)
Al/CuO	1010	1599
Al/WO ₃	1065	1746
Al/Fe ₂ O ₃	1270	1735
Al/Bi ₂ O ₃	857	1098

idea could be extended to oxidizers such as WO₃, SnO₂ and MoO₃, which can produce other gaseous oxidizing species, such as WO₂, SnO, and MoO₃ vapor.

What can be seen in Table 3 is that the experimentally measured ignition temperatures are all above or near to the melting temperature of aluminum (933 K), which as discussed previously, is approximately where nano-Al is experimentally observed to ignite in a gas. Therefore, it would seem that the oxidizer plays an important role in the ignition of nano-Al thermites at high heating rates. In fact, the general trend appears to be that a higher melting temperature results in a higher ignition temperature, with WO₃ being the exception. This does not necessarily imply that melting is a prerequisite for ignition, but suggests that approaching this temperature is necessary for the reaction to become vigorous enough to achieve thermal runaway. To experimentally investigate the reaction in more detail, we next turn to the high heating electron microscopy studies.

3.2. High-heating rate microscopy

For the following discussion, all heating pulses used the maximum heating rate of 10^6 K/s, and the sample always starts at room temperature. The sample is then held at the maximum temperature for a user-specified amount of time (1 ms is the minimum) before the electronics can turn off the voltage. The sample then rapidly cools by a rate governed by heat transfer, and since the substrate is a very small thermal load, this rate is expected to be comparable in magnitude to the heating rate. The parameters which are varied in the following section are the maximum temperature, along with the amount of time the sample is held before the voltage shuts off and quenches the heating. All images are taken at room temperature, and are compared before and after being heated.

Before investigating the thermite systems, a sample of nano-Al with no oxidizer was prepared and rapidly heated in situ within a TEM. The results are presented in Fig. 4, and have also been presented in a previous work [39]. The nano-Al was first given a heating pulse to 1273 K, held for 1 ms, and turned off. Aside from evidence of a minor amount of aluminum crystallization, little morphological change was observed (Fig. 4b). Next, a second heating pulse was employed up to the maximum temperature of 1473 K, and this time the sample was held for 10 ms before the pulse was turned off (Fig. 4c). In this case there was some obvious deformation of several particles, and visual evidence suggesting the aluminum core had migrated outwards. We note that the changes are not very dramatic, and the particles maintain their shapes for the most part. No signs of particle “spallating” were observed at 10^6 K/s, which is approximately the lower limit of where the Melt Dispersion Mechanism is predicted to occur for nano-Al [24]. Finally, the particles were given a heating pulse from room temperature to 1473 K, and this time were held for 1 s before the pulse was shut off (Fig. 4d). In this case, a dramatic change was

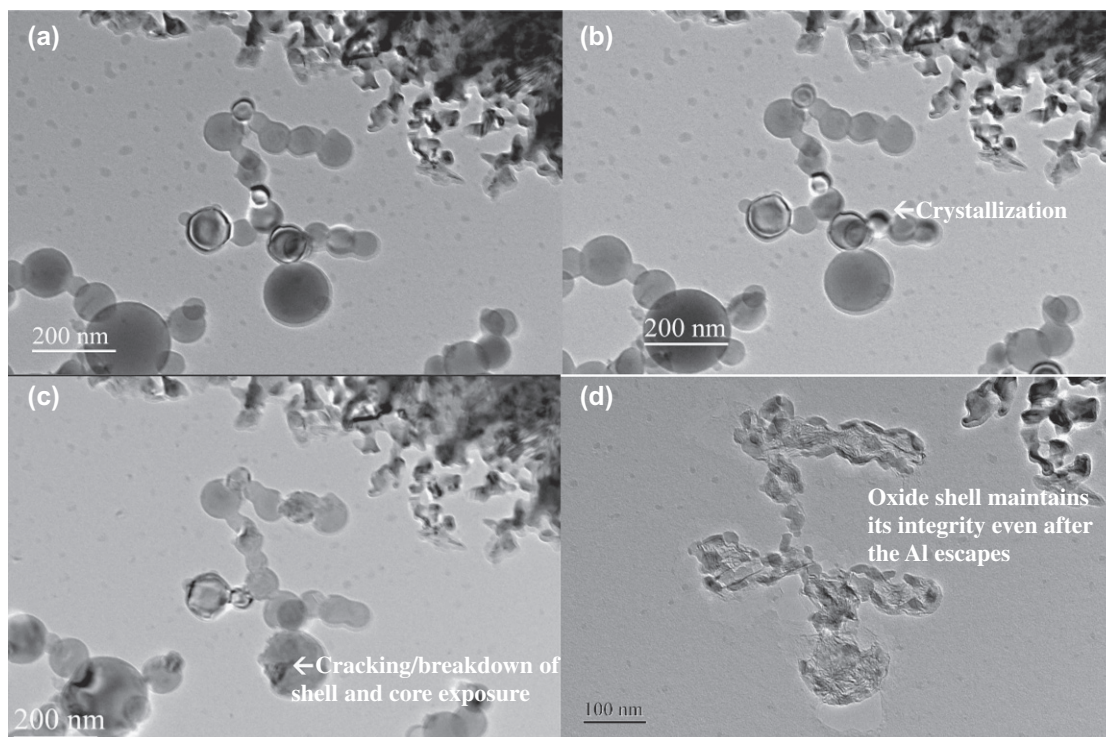


Fig. 4. Nano-Al rapidly heated (106 K/s) via a special holder inside a transmission electron microscope. The heating pulses used as follows: (a) unheated, (b) 300–1273 K, held for 1 ms, off, (c) 300–1473 K, held for 10 ms, off, (d) 300–1473 K, held for 1 s, off. Notice how the oxide shell remains mostly intact, implying that the aluminum has melted and diffused through the shell to escape. There is a possibility that the molten aluminum reacts with the carbon film in (d).

observed in all particles. It was clear that the aluminum had melted and either evaporated or possibly reacted with the underlying thin carbon film to form Al_4C_3 . We do want to point out, however, that the structure of the oxide shell is still visible, indicating that the aluminum core had in some way migrated outwards through the shell during the heating.

Next, we turn to the rapid heating of nano-Al thermites. The first system studied was nano-Al/6nmCuO in the TEM. The small, monodisperse nature of the CuO made it easy to visually distinguish from the larger, polydisperse nano-Al. At the time of this study, the holder had not yet been modified for use with in situ elemental analysis, so the sample was removed and the product was confirmed via elemental analysis in a separate microscope. The heating pulse for this sample was set to the maximum temperature of 1473 K, and held for 10 ms. This particular pulse was chosen primarily based on the observations from Fig. 4, showing that no obvious morphological changes occurred at the lesser heating pulse. The before and after heating images are shown in Fig. 5, and it can clearly be seen that all particles have undergone a dramatic morphological change. The many very fine 6nmCuO particles composing the larger aggregates were seen to form a much larger and nearly spherical single particle of copper as a product. The several large aluminum particles were also found to have sintered into a single oxide product which, unlike the Cu, was not spherical. Another observation is that the fuel and oxidizer have come into surface contact at some point, thus forming an interface. While significant amounts of sintering and morphological changes were visually observed, it was not clear whether the observations were a result of an exothermic reaction, or whether they resulted from the heating.

Next, we investigated the heating of pure CuO to compare with the results of the thermitic. Two samples of CuO were prepared, and were rapidly heated inside a high resolution SEM. In this case, commercially available CuO (Sigma–Aldrich) was used,

simply because the particle sizes are larger and polydisperse, thus giving a broader representation of what occurs. At the time of this experiment, the sample holder had been modified for in situ use with an SEM, therefore allowing for simultaneous elemental analysis. For both samples, the maximum heating rate of 10^6 K/s was used, and the samples were held for 1 ms before the pulse was shut off, however, one sample was heated to 1250 K while the other was heated to 1473 K. Before and after images are shown in Fig. 6. The sample heated to 1250 K showed only mild amounts of sintering, while the sample heated to 1473 K showed a dramatic morphological change. Agglomerates which were several microns in size had completely sintered into much larger “pools” of Cu_2O , confirmed by energy dispersive X-ray spectroscopy (EDS). CuO can decompose according to the mechanism:



The melting temperature of bulk Cu_2O is 1517 K, however, with a wide range of particle sizes present, there will also be some range of melting temperatures. Once melting occurs, the kinetics of sintering are dramatically accelerated, and this point will be revisited later in this work. Another consideration worth mentioning is that sintering is an exothermic event, and this could also serve to self-accelerate the process, causing the particle temperature to rise, and for very small particles (<10 nm), by as much as a few hundred degrees [34]. At high heating rates, this may lead to large amounts of melting even below the bulk melting temperature.

From these results, it is quite clear that the highly agglomerated nanoparticles have sintered into particles with much larger characteristic length scales, and on a timescale faster than 1 ms. The sample was next given a series of subsequent heating pulses, however, the morphology remained unchanged indicating that the melting process had been completed once it was initiated. Comparing these

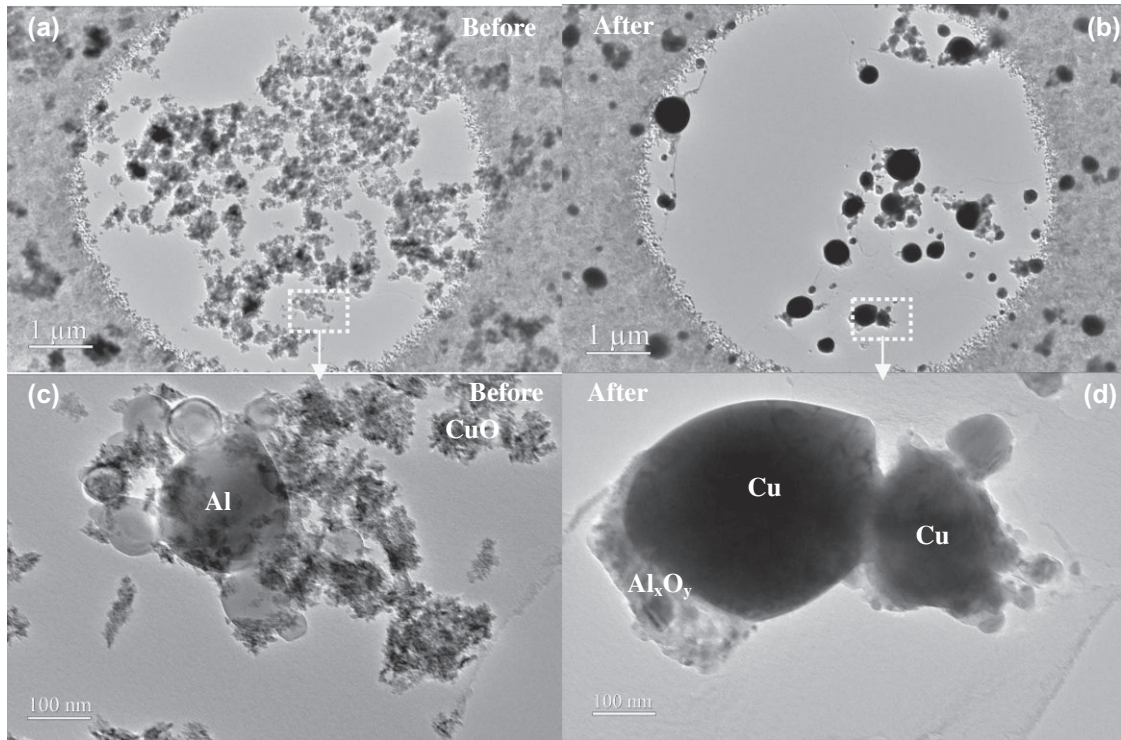


Fig. 5. Before (left) and after (right) images of Al/6 nmCuO rapidly heated from 300–1473 K at 10^6 K/s, and held for 10 ms in a TEM. Images (c) and (d) are higher magnification images of the boxed regions in (a) and (b). The products were separately confirmed by elemental analysis in a separate microscope. The results suggest a reactive sintering mechanism has occurred to produce the observed morphology.

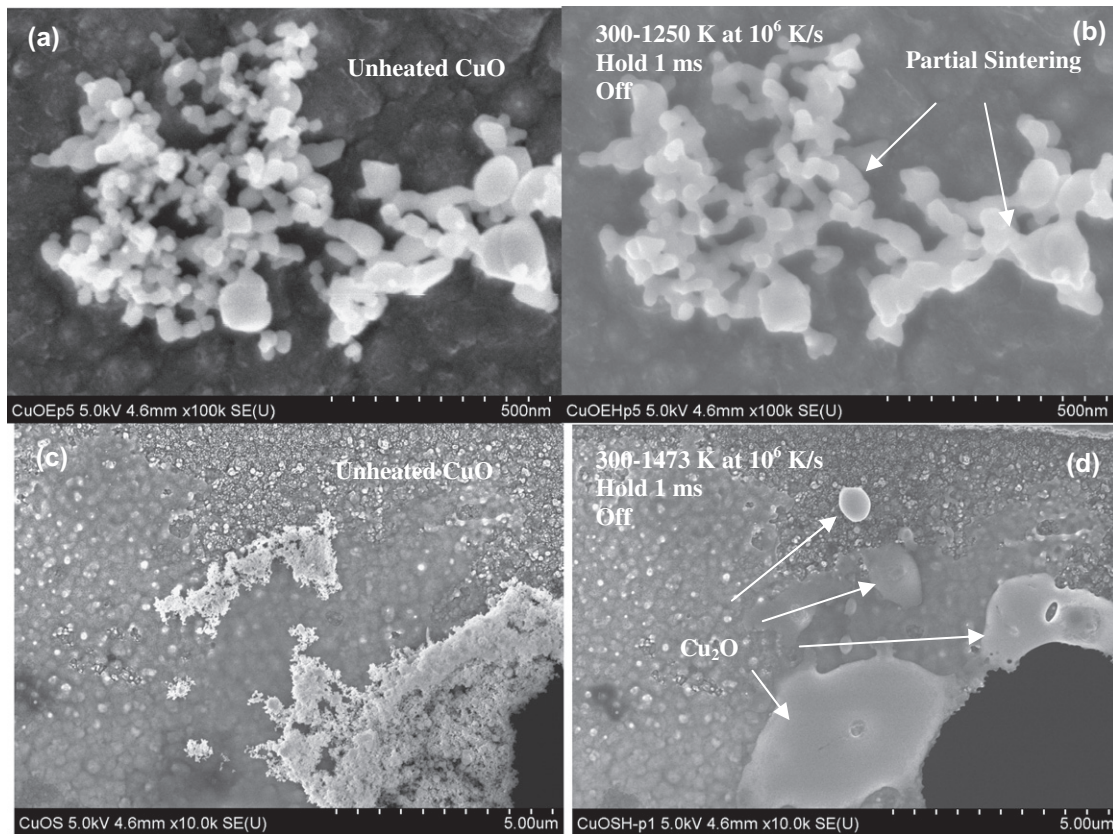


Fig. 6. SEM images of CuO before (a/c) and after (b/d) rapid heating. The top sample was heated to 1250 K while the bottom sample was heated to the maximum of 1473 K. While a small amount of sintering is seen when the sample is heated to 1250 K, the changes are subtle compared to changes observed when heated to 1473 K. Note that the complete sintering of even micron-sized agglomerates occurs very quickly, in this case in a sub 1 ms timescale.

results to the nano-Al/CuO thermite (Fig. 5), we do not observe the formation of spherical copper particles from heating of the pure CuO. What this implies is that the exothermic reaction is indeed occurring in the thermite to further reduce the Cu_2O and produce the Cu product.

In order to render the product morphology seen in Fig. 5, we propose that the Al and CuO have reacted by a reactive sintering mechanism. This terminology has been used to examine the reaction of other systems by various authors [40–43], but to the best of our knowledge has not been reported in metal/metal oxide nanocomposite thermites at this point. In such a mechanism, the fuel and oxidizer aggregates come into surface contact and a heterogeneous reaction initiates at the interface. The heat liberated by the exothermic reaction is conducted away from the interface, and to adjacent particles in the aggregate chains. As material is melted during this process, capillary/surface tension forces serve to rapidly deliver the newly-melted material towards the interface, where the reaction continues. The final morphology depends on the temperature and mobility of the products. In the case of nano-Al/6nmCuO, a large spherical copper product is formed due to the relatively low melting point of copper (MP 1356 K), whereas the high-melting Al_2O_3 (MP 2327 K) product cannot become spherical within the very fast heating (and cooling) of this experiment. It is worth mentioning that, due to this experiment being conducted in vacuum, it is possible that what we observe is actually the reaction between Al and Cu_2O , since CuO decomposes to Cu_2O , which subsequently melts (MP 1517 K). A schematic of the proposed mechanism is shown in Fig. 7.

The next question to ask is whether a reactive sintering mechanism can occur for other thermites, and so we turn to a nano-Al/ WO_3 sample studied in a SEM, some results which have been published [39]. An SEM has the advantage of constructing a back-scattered electron (BSE) image, which is well known to introduce contrast based on atomic weight (higher weight \rightarrow brighter in image). Aluminum and WO_3 can thus be easily distinguished in a BSE image, one reason WO_3 was chosen for this study. The nano-Al/ WO_3 was heated to the maximum temperature of 1473 K, above the experimentally measured ignition temperature (1065 K for nano-Al/ WO_3 , as seen in Table 3). A shortened heating pulse of

1 ms was used in this case in an effort to minimize film stability issues that were seen in the nano-Al/6nmCuO. Also, the burning time from prior optical measurements for nano-Al/ WO_3 was found to be between 1 and 2 ms. Therefore, the goal was to initiate the thermite, and then rapidly quench it 1 ms later by turning of the pulse.

The before and after images of nano-Al/ WO_3 , along with the corresponding BSE images, are shown in Fig. 8. The bright areas in the BSE image correspond to W-containing species, while the dark spots correspond to Al species (separately confirmed by elemental analysis). Unlike the nano-Al/CuO results, an advantage in this study is that the selected area has both the thermite along with the pure oxidizer within the picture, thus allowing for a direct comparison between the two subjected to an identical heating pulse. From Fig. 8, two very different types of behavior can be seen; for fuel and oxidizer in close proximity, evidence of reactive sintering has occurred and the products are found to be in surface contact, while WO_3 , which was isolated from the fuel, shows no morphological changes other than minor amounts of sintering. These observations suggest that the heating pulse alone had not been sufficient to melt the WO_3 ($T_{\text{melt}} = 1746$ K), however, in the areas where the fuel and oxidizer had been intimately mixed, the exothermic reaction had been vigorous enough to further melt the adjacent particles and draw them towards the reacting interface.

The sample was given a second identical heating pulse for an additional 1 ms. The image/BSE image pair after the second heating pulse can be seen in Fig. 9. It should be noted that a large portion of the un-melted WO_3 broke away from the particle, and cannot be seen since this particular image was taken at a higher magnification to emphasize the structure. Also shown in Fig. 9c is an elemental linescan plotting the intensity of W, O, and Al as a function of position (Fig. 9c) across the particles (white line marked in Fig. 9b). The concentration profile indicates that there is some overlap between the species, implying that inter-mixing of the constituents occurs near the interface, an indicator that an interfacial condensed-phase reaction mechanism is happening. In addition, the BSE image (8b) shows the emergence of several small bright “spots,” when compared to Fig. 8d. The spots are likely small

Step 1: Reaction initiates at particle interface. Heat is transferred away from the reacting interface and down the aggregate chains.

Step 2: Newly melted material is rapidly delivered to the reacting interface via capillary/surface tension forces. Gas production may occur simultaneously during this step, i.e. partial oxidizer decomposition or sublimation.

Step 3: Final morphology is material-dependent, and can be affected by the temperature, cooling rate, and local stoichiometry.

Note: Heterogeneous reactions between unburned fuel and gaseous intermediate oxidizers likely occur after or simultaneously with reactive sintering. The relative contribution of reactive sintering and heterogeneous reactions would depend on several factors, i.e. heat transfer, oxidizer decomposition mechanism, local stoichiometry, ion transport, etc.

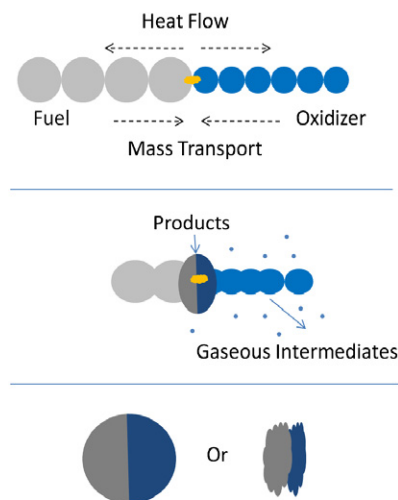


Fig. 7. Schematic of proposed reactive sintering mechanism. For simplicity, the aggregates are shown as linear.

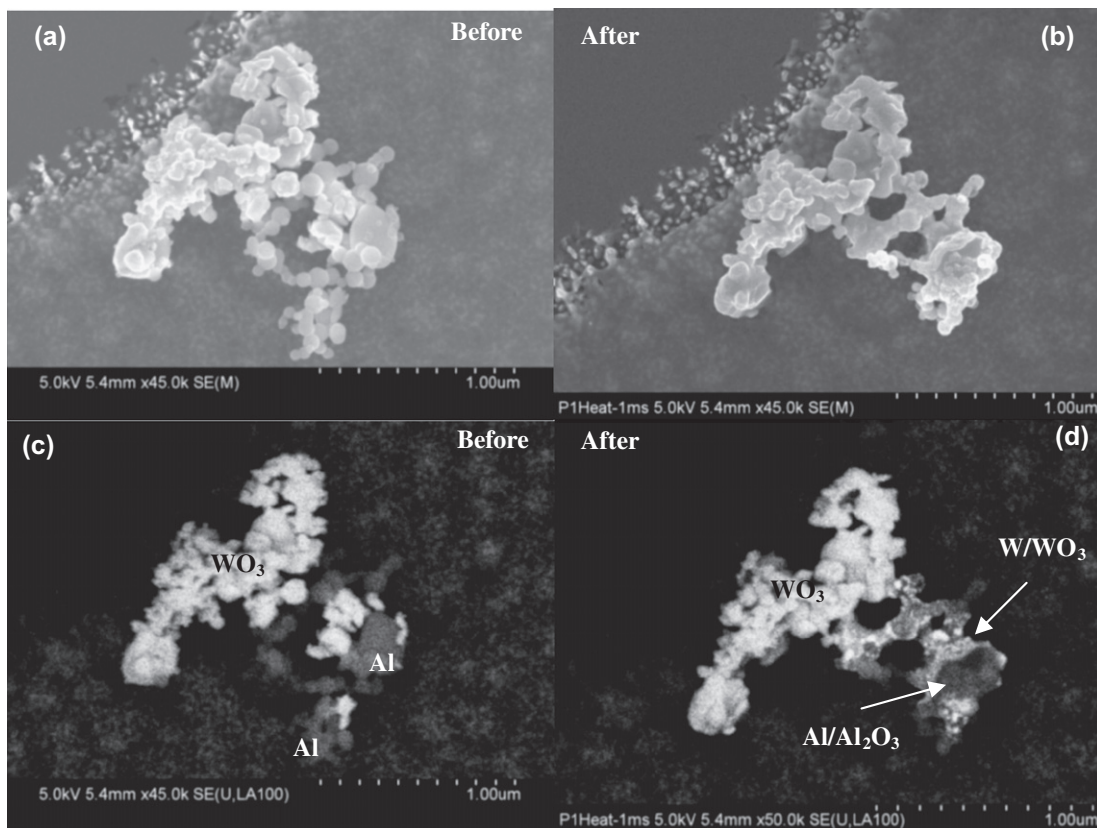


Fig. 8. Secondary electron (a and b) and backscattered electron (c and d) images of a nano-Al/WO₃ thermite sample before (a/c) and after (b/d) heating from 300–1473 K at 10⁶ K/s, and held for 1 ms. The labeled species were separately confirmed using energy dispersive X-ray spectroscopy (EDS). Note that significant morphological changes only occurred in regions where the fuel and oxidizer were closely mixed, indicating that a reactive sintering mechanism drove the melting/fusion of adjacent particles. The WO₃ not in close proximity to Al did not undergo much change, likely because the pulse was not hot enough to melt the WO₃ (MP 1746 K).

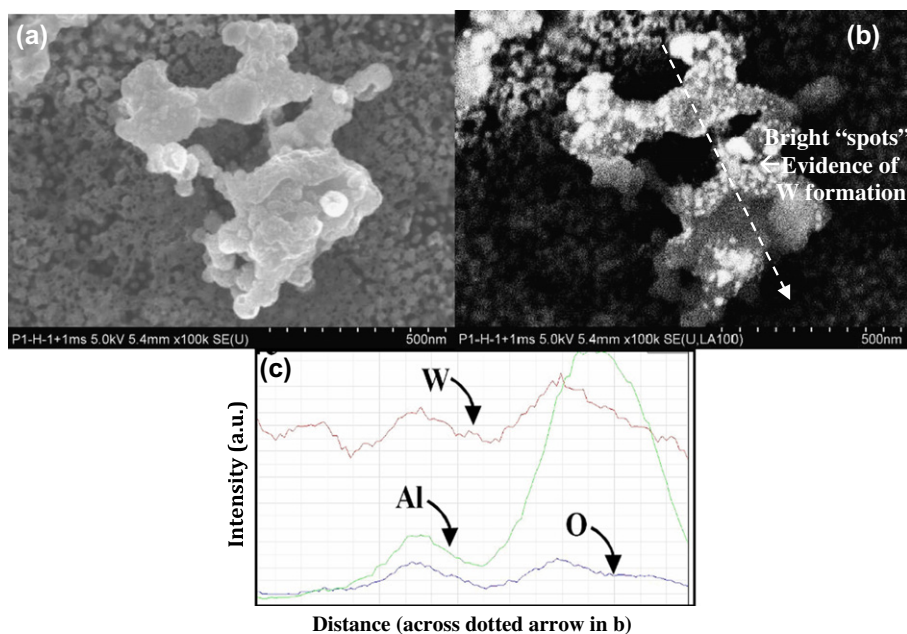


Fig. 9. Nano-Al/WO₃ image/BSE pair (a/b) from Fig. 7, after a second identical heating pulse. Note the formation of small white spots in (b), indicating the formation of solid tungsten as the reaction proceeds. An elemental linescan is shown in (c), which plots the intensity of the W, Al, and O signal as a function of position across the dotted arrow in (b). This linescan indicates that interdiffusion of Al/WO₃ has occurred, indicative of condensed phase reactions at an interface.

clusters of solid tungsten which form during the heterogeneous reaction, and the second heating pulse is allowing for a further extent of reaction. The tungsten product which forms is solid due to

its high melting point (3680 K), and therefore does not render a large, spherical W product. As a comparison, the Cu product previously discussed (Fig. 5) has a low melting temperature (1356 K),

and was found to be spherical. Even if both thermites had reacted by similar mechanisms, the observed morphology will likely differ depending on the temperature and mobility of the products within the timescale of the heating pulse.

To summarize the experimental results obtained from the high-heating microscopy studies, we started by showing that rapidly heated nano-Al exhibited morphological changes consistent with a diffusion mechanism. We next investigated nano-Al/6nmCuO and nano-Al/WO₃ thermites, and suggested that the observed morphologies could be explained by a condensed-phase reactive sintering mechanism. In the nano-Al/WO₃ thermite, a direct comparison of the thermite with pure WO₃ also showed that the exothermic reaction induces a large amount of melting, thus suggesting that oxidizer melting is not a necessary prerequisite for reaction. If reactive sintering is indeed occurring, then ignition would more closely correspond to the temperature where the combined heating from the surroundings and reaction can induce rapid melting of the metal oxide. The ignition mechanism of rapidly heated thermites is the subject of an alternate work.

While the high-heating rate microscopy experiments provide valuable information about the reaction mechanism, there are a few issues worth mentioning. First is the fact that the reaction is in vacuum, and the results may be naturally biased towards observing only the condensed phase reactions. This is particularly important for CuO, which decomposes to release O₂. In vacuum, liberated O₂ may escape from the sample, thus leaving Al only to react with the suboxide, Cu₂O. The other issue is that we are using before and after images to speculate what happened during the very fast reaction. While characteristically larger sintered particles are certainly present in the product, it is not possible from this technique to distinguish whether the sintering preceded reaction, or vice versa. To address these questions, we next turn to the real-time phase contrast imaging of thermites.

3.3. Real-time phase contrast imaging

In this section, high resolution image sequences of samples rapidly heated using the T-Jump/wire setup are presented. The images are created by a real time X-ray phase contrast technique, which provides better structural resolution than traditional X-ray radiog-

raphy. These experiments were performed using synchrotron X-rays from the Advanced Photon Source (APS). The same wire heating T-Jump setup as discussed earlier was used to ramp the temperature of the samples from room temperature to ~ 1500 K at approximately 5×10^5 K/s. Simultaneous optical emission was monitored for the thermites using a photomultiplier tube (PMT). As a preliminary test, rapidly heated nano-Al was investigated, however, no morphological changes were seen to occur other than a small volumetric change as the material slowly melted. Thermites, along with the pure oxidizers, on the other hand, showed very interesting behavior which was imaged with ~ 7.4 μ s time resolution.

Fig. 10 is an image sequence of the nano-Al/CuO thermite being heated on the wire. The images labeled as $t = 0$ μ s correspond to the first image where a morphological change can visually be detected. The particles are seen to lift off the wire, through a propagation process that moves from left to right along the wire. This behavior has been observed in previous work, and has been attributed to the rapid evolution of O₂ gas from the CuO [44]. The onset of optical emission, or ignition temperature, corresponded closely to the frame labeled $t = 0$ in both thermites studied. What is apparent in Fig. 10 is that the formation of characteristically larger structures appears rapidly in time. The exact shape or size distribution of the particles is not something which can accurately be measured due to the limited spatial resolution of the X-ray phase contrast imaging technique (~ 2 μ m), but many of the particle sizes appear to be on the order of micrometers. This behavior is qualitatively consistent with the microscopy results from Fig. 5, where it was shown that sintering of agglomerated nanoparticles led to the formation of larger, nearly spherical particles (~ 1 μ m in some case). Based on this observation, we speculate that the formation of large, more spherical particles in the image sequences corresponds to reactive sintering. The results indicate that evidence of a reactive sintering mechanism can be seen under atmospheric conditions, in addition to under vacuum.

As a comparison, pure CuO was also heated with the same pulse, and the image sequence is shown in Fig. 11. The material was observed to volumetrically shrink, followed by evidence of “bubbling” over the next several milliseconds of heating. These results can be compared to the microscopy results (Fig. 6), where

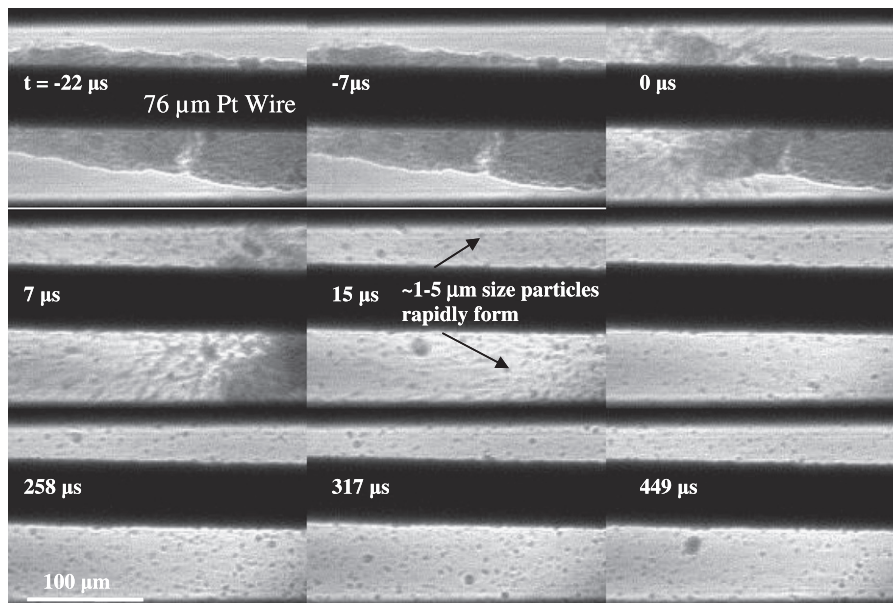


Fig. 10. Series of snapshots of nano-Al/CuO thermite reacted on the wire. Spherical particles with diameters on the order of a few microns were observed to form. The results are qualitatively consistent to the observations in Fig. 5, and suggest the formation of large spherical particles is attributed to a reactive sintering mechanism.

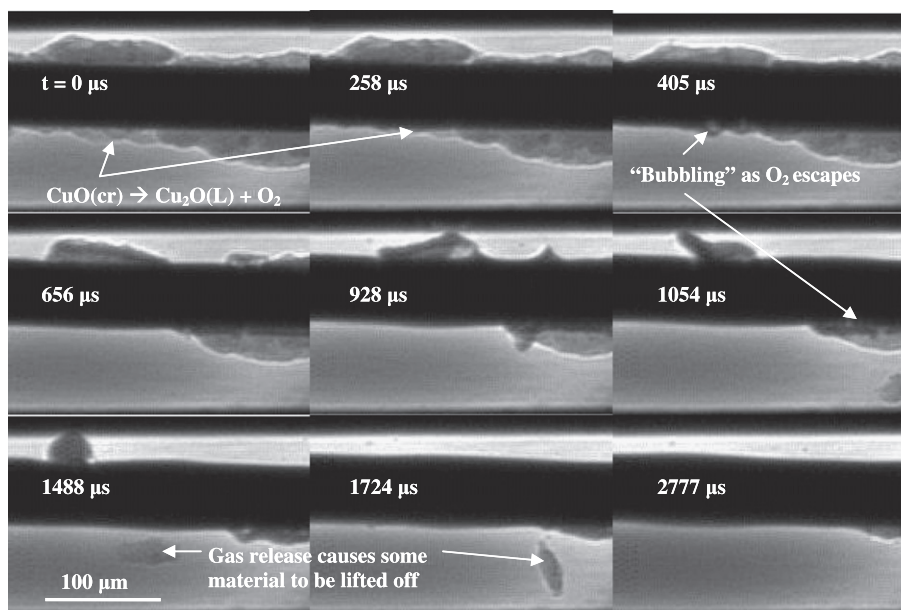


Fig. 11. Series of snapshots nanosized CuO heated on the wire. The video shows signs of “bubbling” indicating that pockets of O_2 are trapped within molten Cu_2O . The gas release causes some material to be lifted off the wire. Overall, the material is removed from the wire much slower than was observed for the thermite.

large agglomerates of nanoparticles rapidly formed “pools” of Cu_2O once a critical temperature was achieved. On the wire, the CuO (cr) decomposes into molten Cu_2O , and simultaneously produces O_2 gas. In the absence of an exothermic reaction, the oxidizer cannot be rapidly decomposed, and thus a large amount of oxygen remains trapped in the condensed phase. The O_2 which was released (or continues to be released via Cu_2O decomposition) is trapped inside the melt and forms pockets of gas as it migrates out through the matrix, experimentally seen as the formation of bubbles within the material.

It is evident from these results that the CuO is indeed releasing O_2 , and thus, is serving as a gas generator. In the presence of an exothermic reaction, oxidizer decomposition is much more rigorous. This serves to finely disperse the powders and lift the material off the wire. What cannot be resolved from this technique is whether the nano-Al heterogeneously reacts with released O_2 gas, or whether it reacts in the condensed phase with the CuO/Cu_2O (L). In fact, it could be a combination of both, and may even lead to a two-step combustion mechanism. Since reaction under vacuum was clearly observed for nano-Al/ CuO (Fig. 5), it shows that at least some amount of reaction proceeds in the condensed phase, since released O_2 gas would escape into the high vacuum, and thus not participate in the reaction.

Next we turn to a thermite with a relatively poor reactivity, nano-Al/ Fe_2O_3 . In a previous work [15], we argued that Fe_2O_3 does not decompose efficiently due to its ability to form condensed-phase FeO , which does not completely dissociate until a temperature (~ 3300 K) even exceeding the adiabatic flame temperature (~ 3100 K). Therefore, it traps a significant amount of oxidizer in the suboxides it produces, even in the presence of an exothermic reaction. The image sequence of the thermite rapidly heated on the wire is shown in Fig. 12. In this case, much larger spherical particles are formed, and some even appear to be hollow. Hollow particles are indicative of gaseous O_2 released into a molten Fe_xO_y matrix, thus forming bubbles, analogous with what was seen for pure CuO in the absence of an exothermic reaction (Fig. 11). Directly comparing the image sequences for the two thermites (Figs. 9 and 11), it appears as though a more intense gas release corresponds to the formation of finer particles. Intense gas release may be beneficial by serving to break apart larger aggregates

and/or agglomerates, ultimately preventing very large, sintered structures from forming.

Although the spatial resolution of the X-ray image sequences is clearly inferior to an electron microscope, the image sequences are especially useful in that the approximate timescale for larger particle formation (sintering) can be visually approximated for the thermites from the image sequences. Using Figs. 10 and 12, the sintering time is estimated as the difference in time between the first visual evidence of a reaction ($t = 0 \mu s$) and when most of the material appears to exist off of the wire as larger particles. This is a very rough approximation, but it is interesting when compared to other measured quantities. The sintering timescale is tabulated in Table 4, along with the full-width at half-max (FWHM) of the optical signal for comparison. It can be seen that the sintering timescale is a much faster process than the burning of the particles, suggesting that significant amounts of sintering may precede much of the reaction.

What is also interesting is that the apparent sintering time for the nano-Al/ CuO is on par with the reported pressure rise time of $10.4 \mu s$, experimentally measured during combustion experiments [15]. In this previous work, we had argued that the pressure rise was evidence of some partial reaction which served to rapidly decompose the oxidizer to release O_2 , followed by prolonged burning in a gaseous oxidizing environment, experimentally seen as a much longer optical signal. The pressure peak occurred well before the optical emission, thus indicating that the pressurization originated from a characteristically low-temperature reaction. From the current findings, we speculate that the reaction may in fact be a two-step mechanism; a fast reactive sintering component between some of the fuel and oxidizer, followed by a prolonged burn as the remainder of the fuel reacts heterogeneously with liberated O_2 . The next section will investigate the timescale of sintering analytically to see how it compares with characteristic reaction timescales.

4. Characteristic reaction and sintering times

Up to this point, we have shown visual evidence that sintering is occurring, however, we have only really discussed it in the context of a reactive sintering mechanism. That is, the exothermic

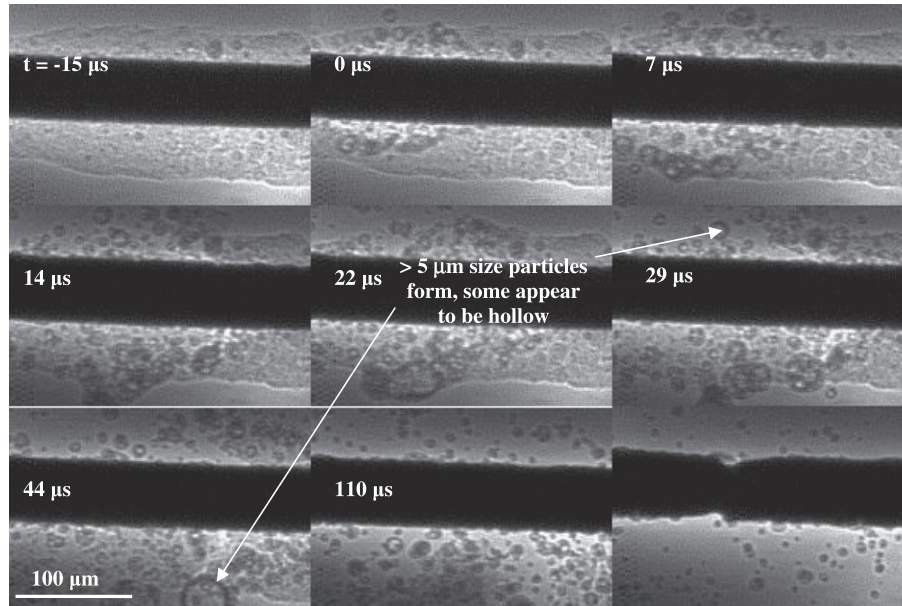


Fig. 12. Series of snapshots of nano-Al/Fe₂O₃ thermite reacted on the wire. Note the formation of micron-sized spherical particles, in this case much larger than was observed for the nano-Al/CuO thermite (see Fig. 9). Some particles appear to be hollow.

Table 4

Various timescales estimated from the movies of the thermites rapidly heated on the wire. Note that in all cases, larger spherical particles form on a faster timescale than when ignition occurs, and much faster than the measured burning times.

Thermite	Approximate time to form larger spherical particles (μs)	FWHM burn time (μs)
Al/Fe ₂ O ₃	44	1900
Al/CuO	15	960

reaction initiates, and this causes rapid melting/fusion of adjacent particles. In general, particle sintering is a thermally activated process, and will occur even in the absence of an exothermic reaction, as long as the temperature is sufficiently high. The following section investigates the kinetic sintering timescale of particles being externally heated, and compares that with a relevant characteristic reaction timescale. Specifically, two relevant examples where the kinetic timescale of the sintering event may be particularly important are:

- (1) Self-heating by convection of intermediate gases in a self-propagating thermite.
- (2) Addition of nanoparticles to a high explosive, where the ambient temperature may rapidly rise to high temperatures (i.e. ~3000 K behind a shock front).

The following section presents a simple estimate of the timescale for sintering of nanoparticles convectively heated by a hot gas, which should be relevant to the two cases above. We chose to ignore the local heat of reaction in this analysis so that the results may be considered an overestimate of the characteristic sintering time.

4.1. Reaction timescale

An estimate of the reaction timescale depends on the particular combustion system and configuration, and for the following analysis, we limit ourselves to our own studies. In a previous work using a combustion cell [15], we showed that the pressure rise oc-

curred on the order of 10 μs, whereas the FWHM burning time was approximately 200 μs. Since we are particularly interested in seeing whether sintering is occurring early in the combustion process, we choose a characteristic reaction time that is a small fraction (5%) of the optically-measured burning time. This leads to a characteristic reaction time of 10 μs, which is coincidentally also the pressure rise time. We ignore particle size effects on burn time for simplicity.

4.2. Sintering timescale

To estimate the sintering timescale, two separate calculations must be included; the time it takes to heat and melt the material, along with the time to actually fuse two particles into one. In a thermite system, there are three materials present; aluminum, an aluminum oxide shell, and the metal oxide. The metal oxide could sinter with other metal oxide particles, or the aluminum may sinter with neighboring aluminum (in which case the temperature where sintering occurs should be somewhere in between the melting point of Al and Al₂O₃). Given that most of the experimental evidence and discussion have focused on the oxidizer, the calculations focus on sintering time of two identical particles of CuO.

To calculate the heating timescale, an approach from a previous work is followed [45]. For simplicity, particles are not treated as agglomerates, but instead as single spheres surrounded by a hot gas, and with radiation losses assumed to be negligible. A lump-capacitance model of heating is assumed, where the heat transfer within the particle is fast relative to the heat transfer between the gas and solid interface, and therefore the particle temperature is uniform throughout at any instance in time. The particle temperature profile is thus governed by the heat transfer from the surrounding gas to the particle, and the rate can be written as:

$$\frac{dT_p}{dt} = \frac{hA}{\rho VC_p} (T_{gas} - T_p) \quad (1)$$

where T_p , A , V , C_p refer to the temperature, surface area, volume, and temperature-dependent heat capacity (calculated with fitting parameters available on the NIST webbook) of the particle, t is time,

and T_{gas} is the surrounding gas temperature. h is the heat transfer coefficient, defined in terms of the Nusselt number (Nu), thermal conductivity of the gas and particle diameter (d_p) as:

$$h = \frac{Nuk_G}{d_p} \quad (2)$$

The Nusselt number of the particles is estimated from the modeling results of Filippov and Rosner [46] for a large gas to particle temperature ratio and accommodation coefficient of 0.3.

For the heating calculation, the gas temperature was assumed to be fixed at 1700 K, just above the melting temperature of CuO (1599 K). This temperature is chosen so as to provide a source of heat to melt the particles (i.e. above the melting point). It should be noted that it is not known what temperature the surrounding gas will be, and in fact it may even be as high as the adiabatic flame temperature (~ 3000 K). Since the experimental results tabulated in Table 4 suggested that apparent sintering occurs fast, we stick with a conservative ambient temperature so it is more likely for us to overestimate the sintering time. Also, the calculations will be even more overestimated since we have ignored the energy liberated via the exothermic reaction.

To calculate the timescale of the fusion process (τ_{fus}), the approach laid out in Mukherjee et al. is followed [35]. Below the melting point, particles can fuse via solid state grain boundary diffusion, whereas above the melting point surface tension forces dominate and the timescale can be estimated by a viscous flow mechanism [47]. Preliminary calculations suggest that the timescale becomes orders of magnitude faster once the melting temperature is reached and the mechanism changes. Therefore, we make the assumption that no morphological changes occur until the particle has been completely melted. Once this occurs, the fusion time can be approximated by:

$$\tau_{\text{fus}} = \frac{\mu d_{\text{eff}}}{2\sigma_l} \quad (3)$$

where d_{eff} is the instantaneous effective particle diameter ($\sim 2d_p$), μ is the size dependent liquid viscosity calculated by an empirical fit [48] (~ 100 mPa s), and σ_l is the surface tension of the liquid (~ 0.7 J/m²) [49].

Eq. (1) was numerically integrated in two steps; time to sensibly heat CuO from room temperature to the melting point, followed by the time to melt the particle at a constant temperature of 1599 K. The latent heat of fusion of Cu₂O was used to approximate the energy required for melting, since this is what CuO decomposes to prior to melting. The heating time is reported as the sum of these two times. Eq. (3) was used to calculate the subsequent fusion time at 1599 K. The heating time is compared with the fusion time in Fig. 13, and as a function of particle diameter. The total sintering time is the sum of the time to heat, melt, and fuse two identical particles with initial diameter d_p . From Fig. 13, it can be seen that the fusion of particles happens on a much faster timescale than the heating time of the particles. In other words, if melting can be achieved then a calculation of the “sintering timescale” of particles can be reduced to a calculation of the time it takes to heat and melt the particles. From these results, we can see that the predicted sintering timescale is comparable to the characteristic reaction timescale. Thus, it is reasonable to expect that sintering processes and their effects (heat release, wetting, change in size, etc.) directly participate in the reaction dynamics of nanothermite mixtures.

As another relevant example of particle sintering timescales, the calculation is extended to the addition of nano-Al to a high explosive, where temperatures can exceed 3000 K, well above the melting temperature of even the oxide shell. The model predicts sintering times that are orders of magnitude smaller than some experimentally measured reaction times, and suggests that, depending on

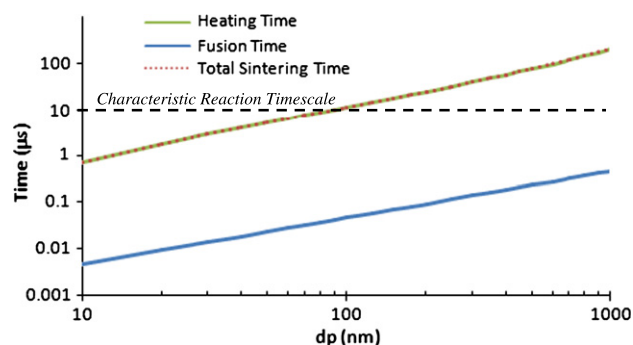


Fig. 13. Model predictions of the total time to sinter CuO nanoparticles in air at 1700 K relative to a characteristic reaction timescale. The total sintering time is assumed to be the sum of two components depicted in the figure; the heating (sensible and latent) time of nanoparticles to the melting temperature, along with the time to fuse the particles calculated by a viscous flow mechanism. The timescale of fusion is found to be much faster than the heating time, therefore, the calculation of the total sintering time can be reduced simply to a calculation of the time it takes to heat and melt nanoparticles. The results show the sintering and reaction timescales are comparable, indicative that a reactive sintering mechanism is plausible.

the particular heating environment, significant sintering may precede much of the combustion. If nanoparticles sinter into larger particle much faster than the characteristic reaction timescale, then this would change our conceptual understanding of how reactivity should scale with particle size. In several examples, authors have experimentally shown a very low diameter dependence on nanoparticle burning times [50,51], even though the burning time in a heterogeneous system has been predicted to scale directly with diameter according to a “ d^1 ” law in this size regime. In many works, however, the designation of particle size is somewhat ambiguous, as nanoparticles are often found to be highly aggregated. If early sintering occurs, then instead of classifying the particle dimensions in terms of the average primary particle diameter or the exposed surface area, it may be more appropriate to calculate the average volume of an aggregate and report the size of an equivalent-volume sphere. Also, experimental techniques which utilize slow heating rates may give different results than high heating experiments. For example, if the reaction of nano-Al in a gas is being studied using thermogravimetric analysis, heat losses may prevent the particle from ever reaching a temperature where sintering can rapidly occur, and thus the particles may maintain their morphologies during the oxidation and display strong size dependence. If, however, nano-Al is shocked to a very high temperature at a high heating rate, the thermal heating alone may serve to melt and sinter particles early, and thus a size-dependence may not be observed.

Collectively looking at all of the experimental results along with the predictions of the sintering timescales, it can be speculated that condensed phase reactions and sintering are occurring early in rapidly heated nano-Al based thermites. While at first it may seem surprising that these reactions may be more prominent than heterogeneous O₂/Al reactions, it becomes plausible when one considers the fast heating/sintering timescale, along with the rapid mass transport of fuel/oxidizer towards each other via a reactive sintering mechanism. Also, very recent work has shown that the reaction between carbon and CuO proceeds largely in the condensed phase [52]. The authors speculate that the decomposition of CuO can be facilitated via condensed-phase reactions, and use density functional theory to examine the decomposition in terms of bond stretching. The results are similar in many ways to what is observed in the current work, but since carbon has a much higher volatilization temperature than aluminum, and does not have a passivating oxide shell, it is not clear whether the mechanisms would be exactly the same.

In this work, we have investigated several different thermite systems at high heating rates, and the results consistently show at least some evidence of reactive sintering is occurring. The ideas presented in this work should help to contribute to both our mechanistic understanding of nano-Al thermites, as well as provide suggestions for design considerations. For example, a highly reactive system may utilize an oxidizer which can readily wet the Al_2O_3 surface to increase the interfacial contact, but also decomposes or transfers the oxidizer rapidly in the condensed phase. Since gas production is important for energy propagation, a volatile product should be formed. Also, the idea of oxidizer size needs to be critically evaluated, since sintering has been shown to dramatically change the morphology early in the reaction. An enhancement in reactivity may not be achieved by decreasing the particle size if the particles do not maintain that size during the bulk of the combustion.

5. Conclusion

This reaction mechanism of nano-Al based thermites using several high heating techniques was investigated. First, thermites were rapidly heated on an ultra thin Pt wire, and the optical emission was monitored to determine the ignition temperature. It was found that three nano-Al based thermites (CuO , Fe_2O_3 , WO_3) ignited above the melting temperature of Al, with $\text{Al}/\text{Bi}_2\text{O}_3$ igniting just below this temperature.

High heating rate microscopy experiments were conducted for pure nano-Al and CuO , along with nano-Al/6nmCuO and nano-Al/ WO_3 thermites. For nano-Al, the results indicate a significant heating pulse was required before large morphological changes were observed. For the thermites, both systems showed evidence that a reactive sintering mechanism involving condensed phase reactions had occurred. The results showed very different behavior for the pure metal oxide than what was seen in region where the fuel and oxidizer were in close proximity, suggesting the exothermic reaction largely drives the sintering process by providing additional heating to rapidly melt the metal oxide.

High resolution image sequences of a thermite of nano-Al/ CuO heated on the wire were collected using a phase-contrast imaging technique, along with images of the pure oxidizer. The results are consistent with the microscopy experiment in that larger, more spherical particles indicative of reactive sintering were observed. It was shown that the CuO is indeed the gas generator, and it is suggested that in the presence of an exothermic reaction, some amount of the oxidizer rapidly decomposes to release gas. A nano-Al/ Fe_2O_3 thermite was also viewed on the wire, and exhibited much larger particle formation, along with evidence of oxygen being trapped and bubbling out over a longer timescale. The results show qualitative differences between thermites with an oxidizer which can rapidly decompose (CuO) vs. one which does not (Fe_2O_3).

Finally, the sintering timescale of CuO nanoparticles was estimated via a simplified model and compared with a characteristic reaction timescale. The results show that the sintering time is comparable to an experimentally measured pressure rise time, suggesting that the burning may be described as a two-step mechanism, reactive sintering followed by heterogeneous combustion with liberated O_2 . The model was also extended for nano-Al heated by hot gases, suggesting that sintering may occur orders of magnitude faster than the complete reaction, a topic which needs further investigation.

All of the results suggest a reactive sintering mechanism is occurring early during the burning of nanocomposite thermites, and the model results suggest that gaseous heating can activate sintering processes on fast timescales, with or without an exother-

mic reaction. Large morphological changes accompany sintering, thus greatly changing the effective particle size early in the combustion. Overall, the results and discussion within this paper provide insight into a condensed-phase reaction mechanism for nanocomposite thermites which can occur on fast timescales.

Acknowledgments

We thank the Army Research Office and the Defense Threat Reduction Agency for their financial support. We acknowledge the support of the University of Maryland's Nanocenter and its NISPLAB. The NISP laboratory is operated jointly by the Maryland Nanocenter and the NSF MRSEC as a shared experimental facility. We also thank Rich Fiore and Protochips, Inc. for their technical help and for supplying the heating holder and grids. We thank Dr. Wen-An Chiou for his help with the operation of the microscopes at UMD. S.T.K. and T.C.H. gratefully acknowledge support from the Office of Naval Research (Grant No. N000014-07-1-0740) for the X-ray phase contrast imaging experiments. Use of the Advanced Photon Source (APS) was supported by the US Department of Energy, Office of Science, Office of Basic Energy Sciences, Under Contract No. DE-AC02-06CH11357.

References

- [1] C.E. Aumann, G.L. Skofronick, J.A. Martin, *J. Vac. Sci. Technol.*, B 13 (3) (1995) 1178–1183.
- [2] D.E. Wilson, K.K. Kim, Combustion of consolidated and confined metastable intermolecular composites, in: 43rd AIAA Sciences Meeting and Exhibit, Reno, NV, 2005, p. 0275.
- [3] J.A. Puszynski, C.J. Bulian, J.J. Swiatkiewicz, *Multifunct. Energetic Mater.* 896 (2006) 147–158.
- [4] D. Prentice, M.L. Pantoya, B.J. Clapsaddle, *J. Phys. Chem. B* 109 (43) (2005) 20180–20185.
- [5] M. Schoenitz, T. Ward, E.L. Dreizin, Preparation of energetic metastable nanocomposite materials by arrested reactive milling, in: *Materials Research Society Symposium Proceedings*, vol. 800, 2003, pp. 85–90 (Synthesis, Characterization and Properties of Energetic/Reactive Nanomaterials).
- [6] K.B. Plantier, M.L. Pantoya, A.E. Gash, *Combust. Flame* 140 (4) (2005) 299–309.
- [7] D.S. Moore, S.F. Son, B.W. Asay, *Propellants, Explos., Pyrotech.* 29 (2) (2004) 106–111.
- [8] J.A. Puszynski, Reactivity of nanosize aluminum with metal oxides and water vapor, in: *Materials Research Society Symposium Proceedings*, vol. 800, 2003, pp. 223–232 (Synthesis, Characterization and Properties of Energetic/Reactive Nanomaterials).
- [9] V.E. Snders et al., *J. Propul. Power* 23 (4) (2007) 707–714.
- [10] M.L. Pantoya et al., *J. Propul. Power* 25 (2) (2009) 465–470.
- [11] S.H. Kim, M.R. Zachariah, *Adv. Mater.* 16 (20) (2004) 1821–1825.
- [12] A. Prakash, A.V. McCormick, M.R. Zachariah, *Nano Lett.* 5 (7) (2005) 1357–1360.
- [13] K.T. Sullivan et al., *Combust. Sci. Technol.* 183 (3) (2011) 285–302.
- [14] K.S. Martirosyan et al., *Nanotechnology* 20 (40) (2009) 405609.
- [15] K. Sullivan, M.R. Zachariah, *J. Propul. Power* 26 (3) (2010) 467–472.
- [16] L.P.H. Jeurgens et al., *Phys. Rev. B* 62 (7) (2000) 4707–4719.
- [17] M.A. Trunov, M. Schoenitz, E.L. Dreizin, *Combust. Theor. Model.* 10 (4) (2006) 603–623.
- [18] J.J. Granier, M.L. Pantoya, *Combust. Flame* 138 (4) (2004) 373–383.
- [19] M.A. Trunov et al., *Combust. Flame* 140 (4) (2005) 310–318.
- [20] A. Rai et al., *J. Phys. Chem. B* 108 (39) (2004) 14793–14795.
- [21] B.J. Henz, T. Hawa, M.R. Zachariah, *J. Appl. Phys.* 107 (2) (2010) 024901.
- [22] V.I. Levitas, M.L. Pantoya, K.W. Watson, *Appl. Phys. Lett.* 92 (20) (2008) 201917.
- [23] V.I. Levitas, M.L. Pantoya, B. Dikici, *Appl. Phys. Lett.* 92 (1) (2008) 011921.
- [24] V.I. Levitas et al., *J. Appl. Phys.* 101 (8) (2007) 083524.
- [25] V.I. Levitas et al., *Appl. Phys. Lett.* 89 (7) (2006) 071909.
- [26] A. Rai et al., *Combust. Theor. Model.* 10 (5) (2006) 843–859.
- [27] V. Rosenband, *Combust. Flame* 137 (3) (2004) 366–375.
- [28] T. Bazyn, H. Krier, N. Glumac, *Combust. Flame* 145 (4) (2006) 703–713.
- [29] T. Bazyn et al., *Combust. Sci. Technol.* 179 (3) (2007) 457–476.
- [30] S. Chowdhury et al., *J. Phys. Chem. C* 114 (20) (2010) 9191–9195.
- [31] M. Schoenitz, S. Umbrajkar, E.L. Dreizin, *J. Propul. Power* 23 (4) (2007) 683–687.
- [32] L. Zhou et al., *Rapid Commun. Mass Spectrom.* 23 (1) (2009) 194–202.
- [33] K.E.J. Lehtinen, M.R. Zachariah, *J. Aerosol Sci.* 33 (2) (2002) 357–368.
- [34] D. Mukherjee, C.G. Sonwane, M.R. Zachariah, *J. Chem. Phys.* 119 (6) (2003) 3391–3404.
- [35] K.J. Blobaum et al., *Acta Mater.* 51 (13) (2003) 3871–3884.
- [36] Y.J. Wang et al., *Nat. Phys.* 4 (4) (2008) 305–309.

- [38] L. Zhou et al., *J. Phys. Chem. C* 114 (33) (2010) 14269–14275.
- [39] K.T. Sullivan et al., *Appl. Phys. Lett.* 97 (13) (2010) 133104.
- [40] Y.B. Liu et al., *J. Mater. Sci.* 46 (4) (2011) 902–909.
- [41] D.J. Roberts, J.F. Zhao, Z.A. Munir, *Int. J. Refract Metal Hard Mater.* 27 (3) (2009) 556–563.
- [42] P. Novak et al., *Int. J. Mater. Res.* 100 (3) (2009) 353–355.
- [43] Q. Zhao et al., *J. Alloy. Compd.* 470 (1–2) (2009) 443–447.
- [44] L. Zhou et al., *J. Appl. Phys.* 106 (8) (2009) 083306.
- [45] K. Sullivan, G. Young, M.R. Zachariah, *Combust. Flame* 156 (2) (2009) 302–309.
- [46] A.V. Filippov, D.E. Rosner, *Int. J. Heat Mass Transfer* 43 (1) (1999) 127–138.
- [47] P. Tandon, D.E. Rosner, *J. Colloid Interface Sci.* 213 (2) (1999) 273–286.
- [48] T. Iida et al., *High Temp. Mater. Processes (London)* 19 (3–4) (2000) 153–164.
- [49] D.A. Firmansyah et al., *Langmuir* 25 (12) (2009) 7063–7071.
- [50] R.A. Yetter, G.A. Risha, S.F. Son, *Proc. Combust. Inst.* 32 (2009) 1819–1838.
- [51] G. Young et al., *Combust. Flame* 156 (2) (2009) 322–333.
- [52] R. Siriwardane et al., *Combust. Flame* 157 (11) (2010) 2198–2208.

Further reading

- [26] V.I. Levitas, *Combust. Flame* 156 (2) (2009) 543–546.